ADVANCED FUNCTIONAL MATERIALS

Supporting Information

for *Adv. Funct. Mater.*, DOI: 10.1002/adfm.202003741

Elastically and Plastically Foldable Electrothermal Micro-Origami for Controllable and Rapid Shape Morphing

*Yi Zhu, Mayur Birla, Kenn R. Oldham, and Evgueni T. Filipov**

Supporting Information

Elastically and Plastically Foldable Electro-Thermal Micro-Origami for Controllable and Rapid Shape Morphing

Yi Zhu, Mayur Birla, Kenn R. Oldham, and Evgueni T. Filipov[*]

Table of content:

This pdf file includes

Other supplementary materials for this manuscript include the following:

S1. Fabrication details

This section gives a detailed description of the fabrication process, including comments and suggestions on the selection of process parameters that may be useful for the readers working to replicate this work. As needed, it may be necessary to adjust the process to compensate for different equipment settings.

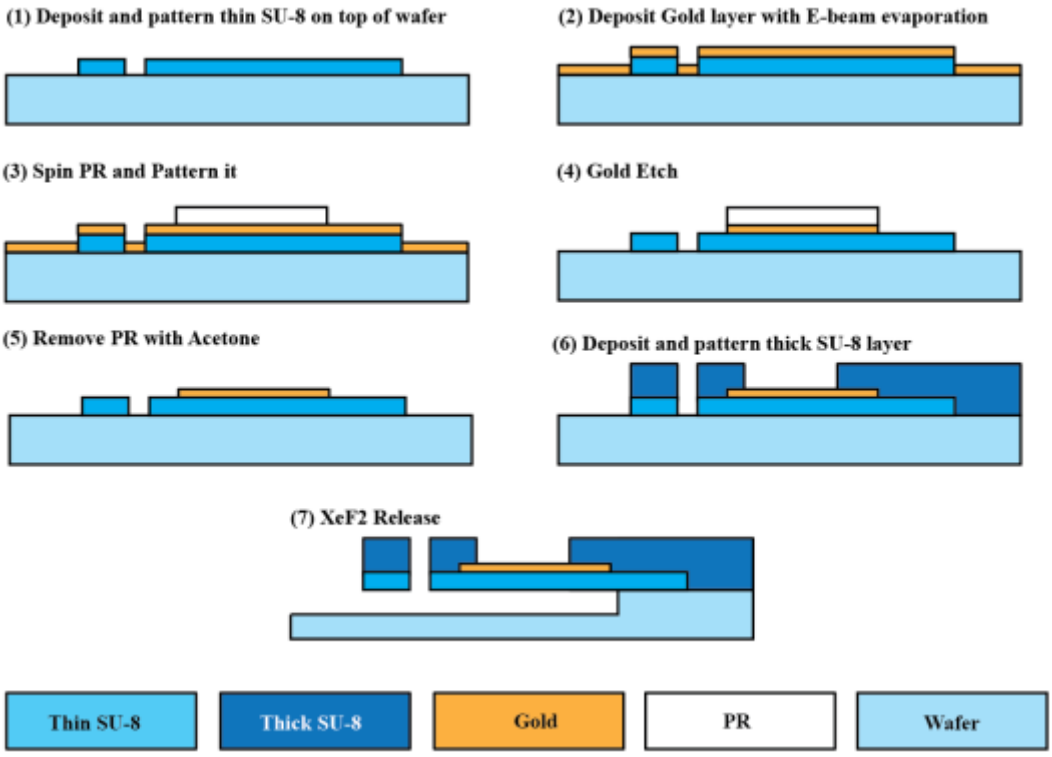

Figure S1. Summary of the fabrication process

Figure S1 gives a detailed process summary. This process starts with spinning a thin film SU-8 2000.5 resin (0.8 μm) on top of a bare Si wafer. Because the SU-8 2000.5 resin is a very fine and thin solution, it is difficult to maintain a nice and even film directly on top of the bare Si wafer. Thus, mild oxidization is recommended to improve the film condition. We apply 20 sec of O2 plasma etch on the Si wafer to promote the adhesion and this allows us to obtain an even SU-8 thin film. Next the SU-8 thin film is soft baked for one minute and patterned with standard mask aligner. The exposure time can be calculated according to the

datasheet provided by the manufacturer[1]. Hard contact mode or equivalent is recommended for better pattern transfer. We recommend adding an extra dosage of exposure in addition to the recommended time from the data sheet to improve the adhesion. After the exposure, one minute of post exposure baking and 90 sec of developing is used to remove the unexposed SU-8.

A thorough hard bake is necessary to ensure that the SU-8 is fully cross-linked. However, overheating the thin film SU-8 can change its residual stress profile and results in unwanted residual curvatures. Based on our experience, a long hard bake at a relatively low temperature produces a better result. For the structures fabricated and tested in this work, we performed an overnight hard bake at 70 degree centigrade.

Next, we deposit the gold layer on top of the thin film SU-8 by e-beam evaporation. To promote the adhesion between the gold and the SU-8, we first add a 0.01 μm layer of chrome under the gold. The gold layer is masked by common photoresists such as SPR 220 and patterned with standard wet etch (see section S2 for thickness selection of the gold layer). It is necessary to perform a short O_2 plasma etch immediately before the wet etch to promote the quality of etching. After the wet etch, the masking photoresists can be removed with IPA and Acetone. This removal will not damage the thin film SU-8 because SU-8 is not dissolvable by IPA or Acetone.

After patterning the gold, we deposit a thicker SU-8 layer to fabricate the panels. We spin coat a 20 μm thick layer of SU-8 2010 onto the wafer. The spin speed is determined according to the data sheet provided by the manufacturer[1]. Similar to the thin film, we patterned this thick SU-8 with standard photo-lithography equipment with a hard contact mode. To ensure good adhesion between the thick SU-8 layer and the existing layers, we recommend extending the exposure time slightly based on the data provided by the manufacturer. This extra time helps to resist the peeling off during the developing of SU-8. Moreover, we recommend not to use IPA for rinsing and only use the SU-8 developer to

further avoid peeling off. Finally, the structure is released with a Xenon Difluoride etch machine. We placed 40 μm wide etch holes in a square grid at 120 μm spacing. These holes are sufficient to release the system from the silicon substrate.

One of the major issues when fabricating small-scale structures is to control and mitigate the influence of residual stresses. In the proposed method, among other functions the gold layer also serves to control the residual stress which induces initial curvature as shown in Figure S2. The thin film SU-8 has a tendency to bend upward after released due to the gradient residual stress across thickness. Thus, by putting the patterned gold layer on top of the SU-8, we can strengthen the surface and thus prevent this initial curvature from happening. We have also found that putting the gold layer under the thin SU-8 can trigger unwanted residual stress as shown in Figure S2 (b). This unwanted residual stress makes it more challenging to create actuators that bends downward. Instead, we use a combination of active folds and passive folds to solve the above issue, which is demonstrated in detail in Section 2.4 of the main article.

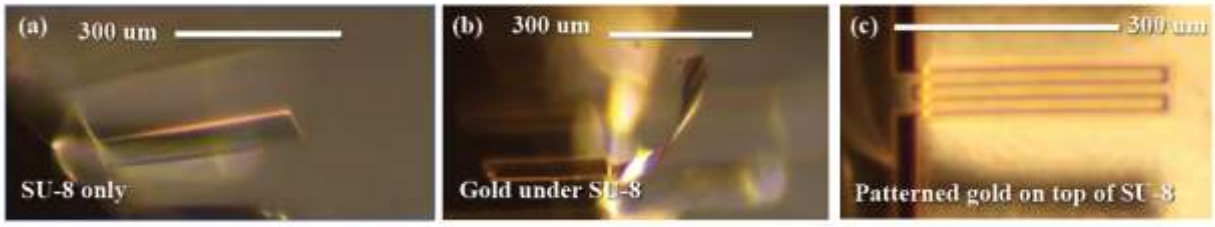

Figure S2. Residual stress and curvature of released systems. (a) Slight curvature with no gold layer. (b) Large curvature when gold is placed under SU-8. (c) No curvature when gold is on the top of SU-8.

S2. Estimating folding angle of the bimorph actuator with Timoshenko's beam model

The design of the gold-SU-8 electro-thermal bimorph actuator is introduced in detail in the main article. Here, we introduce a simple model proposed by Timoshenko[2] that can be used to estimate the folding behavior of the proposed actuator system. This particular model is

used to analyze various types of bimorph active actuator systems such as those in[3]. The curvature of the bi-material beam under elevated temperature can be calculated as:

$$\kappa = \frac{6(\alpha_s - \alpha_g)\delta T(1+m)^2}{h\left(3(1+m)^2 + (1+mn)\left(m^2 + \frac{1}{mn}\right)\right)},$$

where the notations used are defined as the follows: α_g and α_s are the thermal expansion coefficient of the gold and SU-8 layers; $m = t_g/t_s$, where t_g and t_s are the thickness of gold and SU-8 respectively; $n = E_g/E_s$, gives the ratio of Young's modulus of the two materials; h is the total thickness of the bimorph and $h = t_g + t_s$; δT is the elevated temperature of the bimorph actuator.

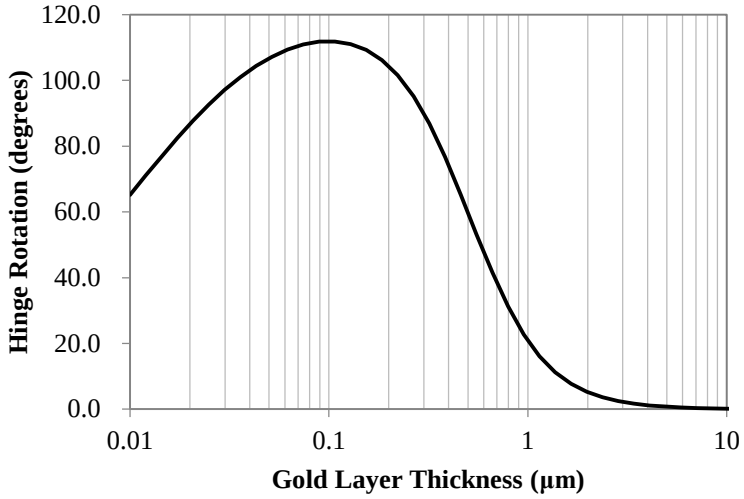

Figure S3. Beam rotation of a 400 µm long actuator beam with varying gold thickness. (Thickness of SU-8 is fixed at 0.8 µm, differential temperature fixed at 80 K)

To optimize the thickness of gold, we fix the thickness of the SU-8 layer to be 0.8 µm and vary the thickness of gold to find a thickness that gives the largest curvature. The Young's modulus of gold is assumed to be $E_g = 79$ GPa and the thermal expansion coefficient is $\alpha_g = 14$ ppm K^{-1}. We manually reduce the Young's modulus of gold by half because gold only covers about half of the actuator area. The material properties of SU-8 are

assumed as the following: Young's modulus of $E_s = 2$ GPa and thermal expansion coefficient of $\alpha_s = 52$ ppm K^{-1}[4]. The elevated temperature used is set as 80 K and the results are given in the Figure S3. The curvature is converted into the rotation of a 400 μm beam for more intuitive understanding. The conversion between rotation and curvature is: $rotation = l\kappa$, where $l = 400$ μm is the beam length. As shown in Figure S3, a gold layer of around 0.1 μm thickness can give the maximum rotation. For the final design, a 0.2μm thick layer of gold is selected for better robustness without significantly changing the folding behavior.

S3. Testing the performance of single-crease origami at different temperatures

This section introduces how we test the folding performance of the single-crease origami at different temperatures. First, we introduce how we package the small-scale origami systems tested in this work. When designing the masks, we create relatively large (3 mm × 3 mm) gold pads on the wafer so that we can directly solder thin electric wires to provide the input current. Before the structures are released, we dice the wafer into smaller pieces so that they are easier to handle. We then use metal boxes as containers because these small-scale origami are sensitive to the electro-static forces generated by the electric charges in polymeric containers (Figure. S4 (a)).

A small mirror is used to provide a side view of the single-crease origami samples (Figure. S4 (a)). This mirror allows us to directly measure the folding angle of the single-crease origami based on the camera pictures we take during the tests. The electric wires are connected to a DC power source (or an AC power source) to provide and measure the input voltage and current.

Figure S4 (b) and (c) show the devices we used to change the environmental temperature. A hot plate is used to generate temperature that is higher than the room temperature. Foam walls are used to make an insulated compartment for testing. We fabricated a small circular lid from acrylic to cover the compartment so that a stable thermal

environment is obtained. An ice bath is used to generate the temperature that is lower than the room temperature.

In this work, we created the large pads to solder electric wires onto wafer for convenience. However, this is not the most efficient way of packing these small-scale active systems. In real practice, it is possible to use much smaller pads (100 μm × 100 μm) and use wire bonding machines to connect thin gold wires to power these systems. With the wire bonding technique, we can pack many more small-scale origami on a single wafer and thus reduce the price of a single device. The mask design we used in this work generally creates about 25 different origami on a single 4" silicon wafer, because the large gold pads for soldering consume large areas on the wafer. We estimate that it is possible to increase the number of devices by a factor of five if we eliminate these large pads.

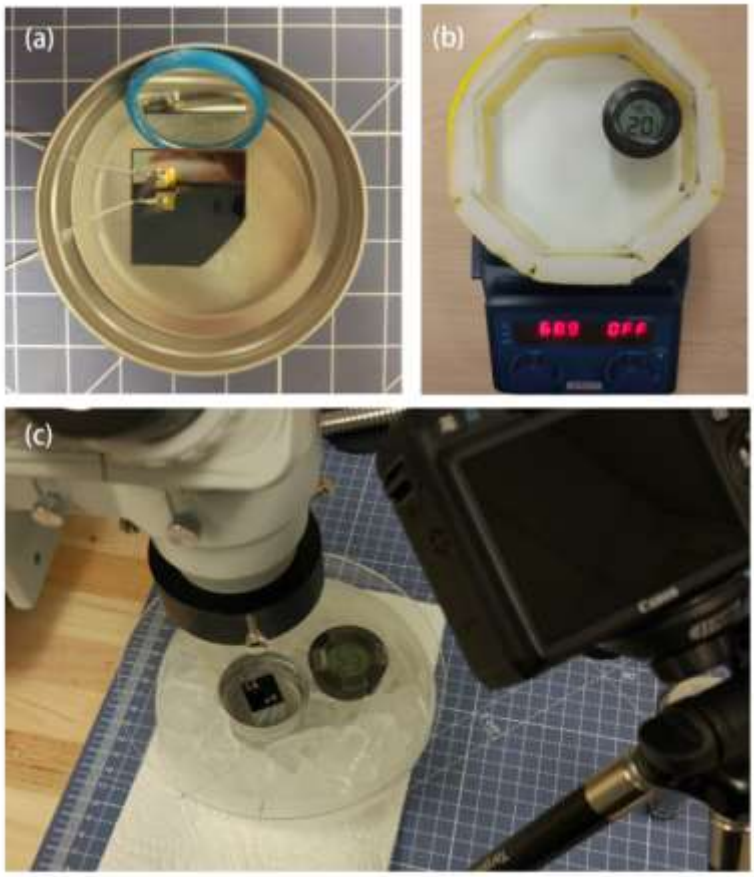

Figure S4. Devices for testing the performance of a single-crease origami (a) metal container with mirror; (b) temperature controlled compartment on hotplate; (c) Full system set-up with ice bath.

For each data point presented on Figure 2 (a), (b), and (d) in the main text, the following loading scheme is used to measure the fold angle and the current. This loading scheme is a 0.1 Hz square wave lasting for one minute with a total number of 6 cycles. No significant variation is observed during the tests between each cycle. (The video presented in video S1 uses a square wave with shorter period for demonstrating purpose.)

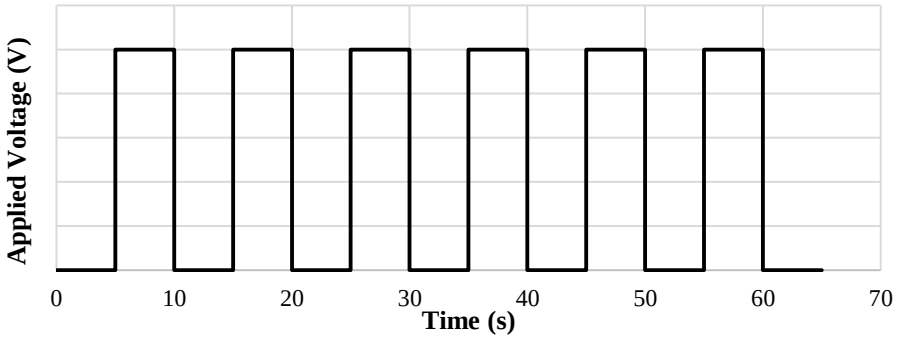

Figure S5. Loading scheme used to measure the current and fold angle of single-fold origami

S4. Analytical model to estimate the resonance frequency and blocking moment

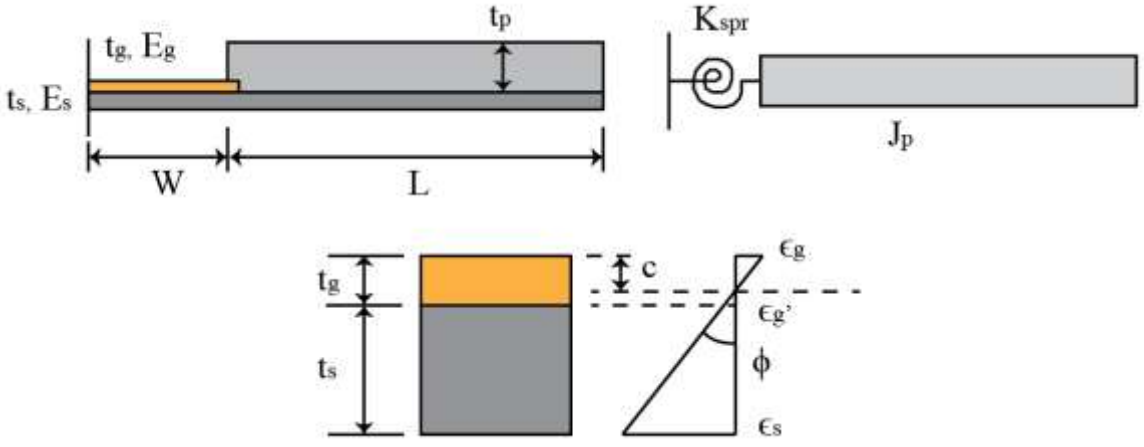

Figure S6. A one degree of freedom model to estimate the resonance frequency

This section introduces a one degree of freedom analytical model that can be used to estimate the resonance frequency and blocking moment of the single-crease origami. We simplify the single-crease origami system as a one degree of freedom mechanism with a rotational spring of stiffness K_{spr} and a panel with the moment of inertial about the spring as J_p. Geometries and material properties used to calculate the stiffness and the moment of inertia are listed on Figure S6. We have:

$$t_g = 0.2\ \mu\text{m},\ \ E_g = 79\ \text{GPa},\ \ t_s = 0.8\ \mu\text{m},\ \ E_s = 2\ \text{GPa},$$

$$W = 200\ \mu\text{m},\ \ t_p = 20\ \mu\text{m},\ \ L = 1\ \text{mm}.$$

We assume that the depth of the structure is 1 (dimension perpendicular to the page) and assume that the plane section of the bilayer beam remains plane after deformation, which is a conventional assumption used in small-strain beam theory[5]. We further assume the density of SU-8 to be $\rho_s = 1200\ kg/m^3$, which will be used to calculate the moment of inertia of the panel.

We first calculate the bending rigidity of the bimorph actuator. We assume that the neutral axis (the term c) is in the gold layer and assume that the material response is linear elastic. We reduce the Young's modulus of gold by a factor of two because the heaters only cover about half the area of actuator. The equilibrium of forces requires:

$$\frac{1}{2}\epsilon_g c E_g = \frac{1}{2}\epsilon_g'(t_g - c)E_g + \frac{1}{2}(\epsilon_s + \epsilon_g')t_s E_S$$

$$\epsilon_g = \phi c,$$

$$\epsilon_g' = \phi(t_g - c),$$

$$\epsilon_s = \phi(t_g + t_s - c)$$

We use the above equations to solve for the location of neutral axis and obtain $c = 0.184\mu m$. Thus, the neutral axis is in the gold layer and the above calculation is valid. We can compute the bending rigidity to be:

$$EI_{comp} = \frac{1}{3}E_g c^3 + \frac{1}{3}E_g(t_g - c)^3 + \left(c + \frac{1}{2}t_s\right)E_s(t_g - c)t_s$$

$$+\frac{1}{2}\left(c + \frac{2}{3}t_{su}\right)E_s t_S^2 = 5.56 \times 10^{-10}\ N \cdot m$$

We can then convert the bending rigidity of beam to the stiffness of the rotational spring with the pseudo-rigid-body model[6] as:

$$K_{spr} = \frac{EI_{comp}}{W}$$

The moment of inertia of the panel is:

$$J_p = \frac{1}{12}\rho_s(t_p + t_s)L \cdot L^2 + \rho_s(t_p + t_s)L\left(W + \frac{1}{2}L\right)^2$$

$$= 1.43 \times 10^{-11}\ kg \cdot m$$

Also, because half of the area of the actuator crease region is occupied by the releasing holes, we further reduce the spring stiffness by half to consider the reduction in stiffness (see Figure 1. in main text). Thus, the fundamental frequency of this one degree of freedom system is calculated as follows:

$$\omega = \sqrt{\frac{K_{spr}}{2J_p}} = 311.8\ rad/sec$$

$$f = \frac{\omega}{\pi} = 99\ Hz$$

Despite the simplicity of this one degree of freedom model, we observe that this analytical value is higher than but close to the 75 to 82 Hz resonance frequencies recorded in the experiment. One reason for the overestimation is that at elevated temperatures, the polymer material becomes softer and thus results in a longer natural period (lower natural frequency). Besides, because we impose strict restriction on the panel deformation and assume that the panel is rigid, we are overestimating the stiffness of the system, which likely accounts for part of the difference in resonance frequency. Also, the above model does not consider the influence of damping on the fundamental frequency. Including the damping

effects can further reduce the resonance frequency of the system. A more elaborate FEM simulation with dynamic solver that considers the electro-thermal-mechanical coupled behavior and the visco-plasto-elastic material response of the system can produce a result with higher accuracy, but this detailed modeling is beyond the scope of this work.

We have also studied the blocking moment of the single-crease origami using this analytical model. The blocking moment is defined as the moment for a given elevated temperature that prevents the bimorph actuators from folding (no deformation). Timoshenko's bimaterial beam model[2] gives an equation to calculate the curvature (κ) of the actuator as was presented earlier in section S2. With the calculated EI_{comp} the blocking moment for a given elevated temperature is:

$$M_{block}(\delta T) = EI_{comp}\kappa(\delta T).$$

This relationship between the elevated temperature and the blocking moment is shown in Figure S7. We can also calculate the downward gravity induced moment acting on the structure. We can see that the actuator system needs to first overcome the gravity induced negative folding before producing the positive upward folding. Because of the Si wafer underneath the folding panels, the negative folding is not observable. Therefore, when the input current is low, the single-crease origami remains in contact with the substrate and no folding occurs.

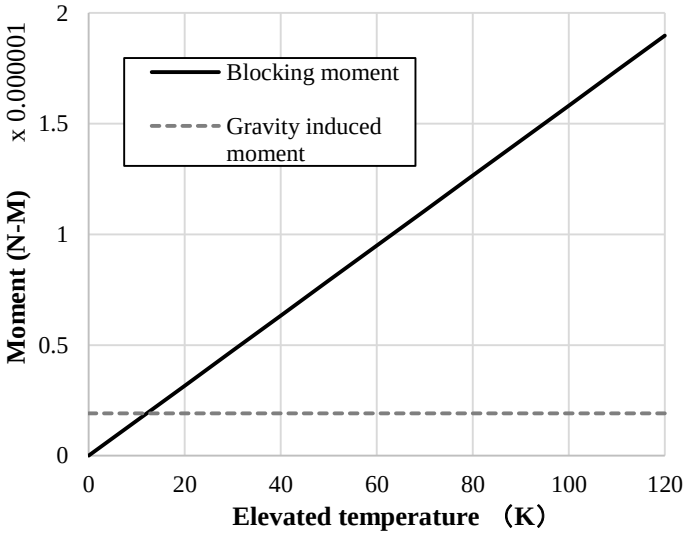

Figure S7. Relationship between the blocking moment and elevated temperature.

These results indicate that more advanced simulation methods are required to fully understand the behavior of these folding systems under the influence of gravity and other complex issues such as the changing thermal boundary. These more advanced simulation methods will enable us to explore the limits of these electro-thermal micro-origami and come up with appropriate designs to avoid misfolding without relying on a trial and error based methods.

S5 Extended cyclic loading performance and long-term behavior

To study the extended cyclic loading performance, we test a single-crease micro origami with a 300 μm long actuator under cyclic oscillation at the resonance frequency of 55 Hz for 30 minutes and record how its minimum fold angle and maximum fold angle change over time. Figure S8. shows the measured results where only minor degradation in performance occurs. The minimum fold angle remains unchanged throughout the testing and the maximum fold angle increases by only a few degrees from the beginning to the end of the experiment (from about 83° to about 86°). Overall, this slight increase in maximum fold angle is minor

compared to the total range of the actuator. During the entire cyclic experiment, this single-crease origami sample has experienced 99000 cycles of folding and unfolding.

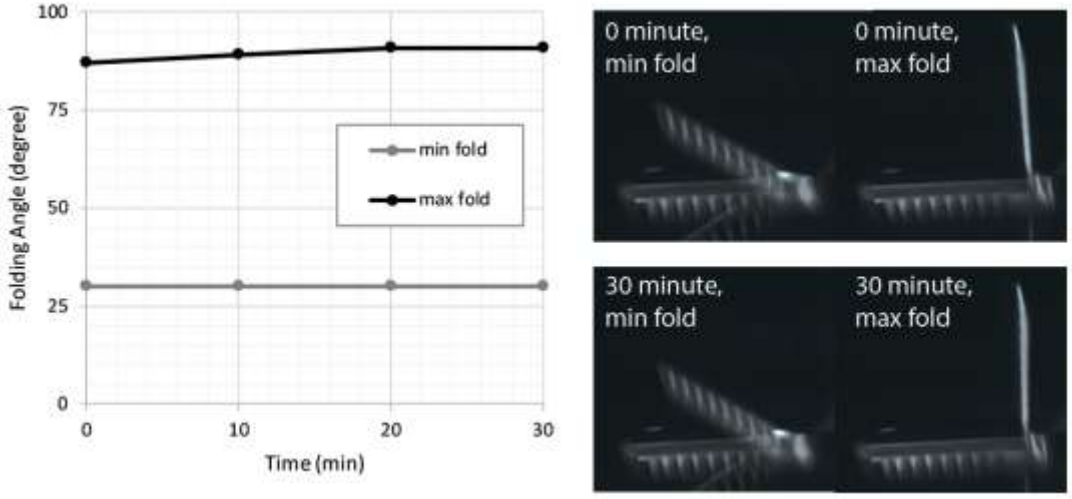

Figure S8. Degradation of the folding range is minor after 99000 cycles of folding and unfolding.

We have observed that these single-crease origami will develop positive folding over long durations of time. During the 3 to 4 months of the manuscript preparation, submission, and review process, we found that these single-crease origami had developed about 10 to 20 degrees of folding in the upward direction. We suspect that this folding is potentially due to the swelling effects of SU-8 absorbing water from atmosphere (it had been a relatively wet spring season and the AC at our lab is mostly running at reduced power level during the March – June 2020 COVID-19 lock down). The swelling induced expansion of SU-8 has been documented in [7]. However, this swelling induced expansion did not create any major issue for us to perform additional experiments, because we could use the plastic folding to offset this long-term folding first and then perform the new tests. We observed no obvious difference between the new tests and the original tests, (e.g. single crease origami tests in Figure 2 of main text) highlighting the potential durability of the proposed system. However, we believe more elaborate experiments are needed to study these long-term effects.

5. Supplementary videos

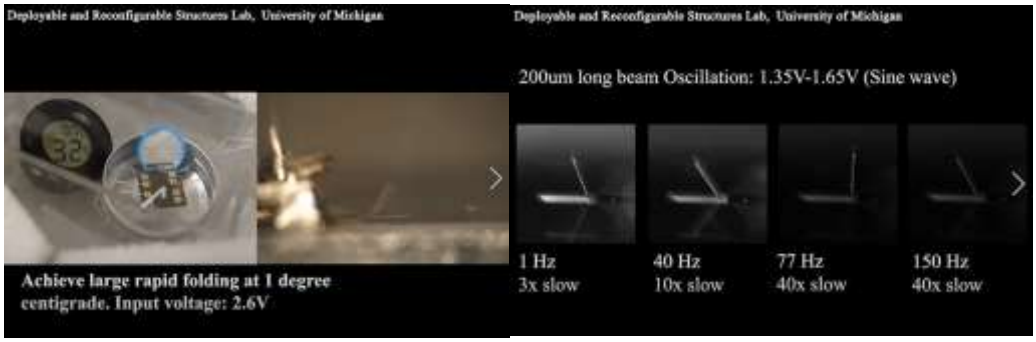

Video_S1_ElasticFolding

In this video, we summarize the results of testing the elastic folding ability of the single-crease origami system. First, the video shows the single-crease origami folding at approximately 1°C, 23°C, and 49°C. In these tests, we use a single-crease origami with 300 μm long actuator beams and control the input voltage to be relatively low such that the folding is elastic. We vary the input voltage and record the corresponding folding angle. The relationship is summarized in the main text. The second half of the video shows the dynamic loading results of the single-crease origami. In this test, we use the same single fold pattern with 200 μm long actuator beams and input a sine wave that oscillates from 1.5 V to 2.5 V. We gradually change the input frequency from 1 Hz all the way to 200 Hz. The video shows that the system can fold rapidly even at high frequencies. At the resonance frequency of about 80 Hz, the system can fold from 10 degrees to 60 degrees reversibly, which is faster than most current systems that can accomplish large folding angles [3].

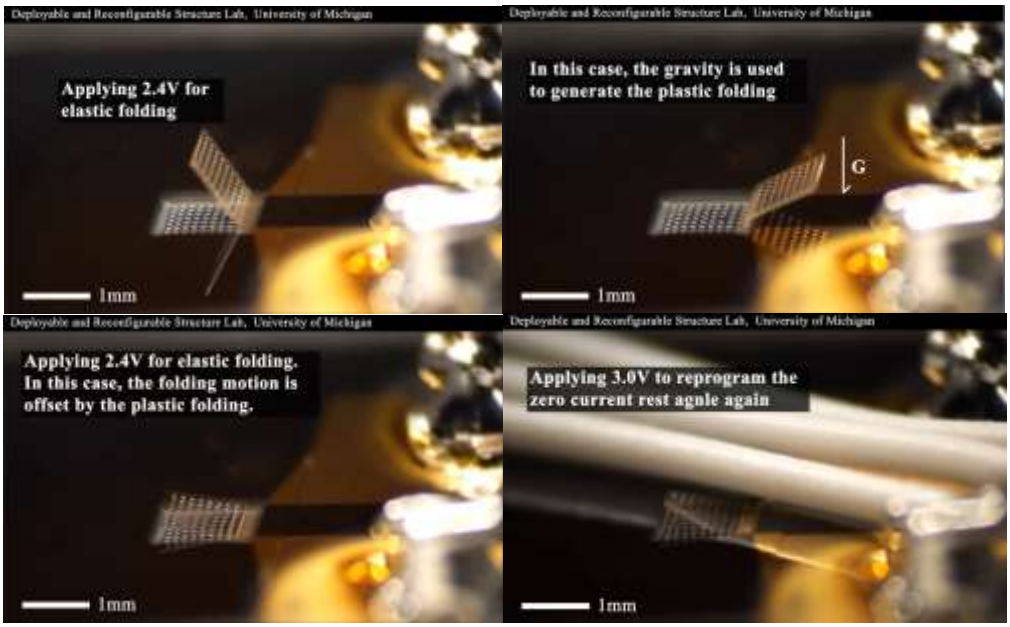

Video_S2_PlasticFolding

In this video, we show how we can achieve plastic folding by reprograming the zero current rest angle of the folding creases. We test a single-crease origami with a 200 μm long beam and the process is summarized in the Video S2. First, we show that by applying a 2.4 V input, the system can fold reversibly in an elastic manner. Next, we apply 3.0 V to the single-crease origami so that the system develops a residual plastic deformation of about 10 degrees under the influence of gravity. When we apply the 2.4 V input after the reprograming, we find that the elastic folding range is offset by the plastic folding by approximately 10 degrees. We use the thin electric wires to press down the panel and reapply the 3.0 V, such that we can reprogram the zero current folding angle and recover the original condition. Two control tests are performed to verify the findings. First, we change the direction of gravity by hanging the wafer vertically and applying the 3.0 V. In this case, we found that the gravity no longer generates the plastic folding because it acts to re-center the crease back to the flat state. Next, we use an electric wire to hinder the recovery motion after overheating the single fold. Because the crease is still hot as it folds back, we can develop more plastic folding by hindering the motion.

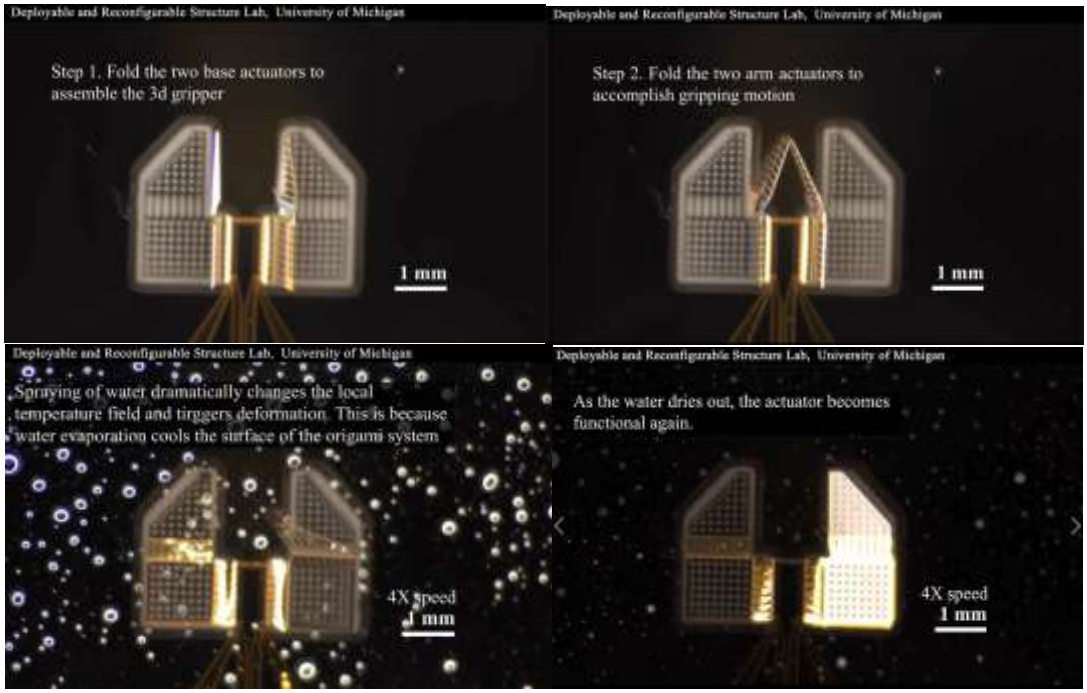

Video_S3_2DofGripper

In this video, we demonstrate a 3D gripper design with two degrees of freedom that can achieve millimeter range gripping motion and can survive a wet environment. This result demonstrates the usefulness of using a micro-origami system with multiple active degrees of freedom to achieve a "fold and function" active system. First, we can fold the gripper by applying a current through the assembly circuit that folds the two anchor panels to the vertical position. Next, we can apply a current through the functioning circuit to close the two arms to grip. If we release the applied current, we can recover to the flat configuration. After the structure recovers the flat configuration, we sprayed water on to the substrate. After spraying the water, the thermal profile changes dramatically due to the water evaporation. The water evaporation triggers unwanted folding in the system, but the effect dies out as the water dries. After the water dries, the system functions normally again.

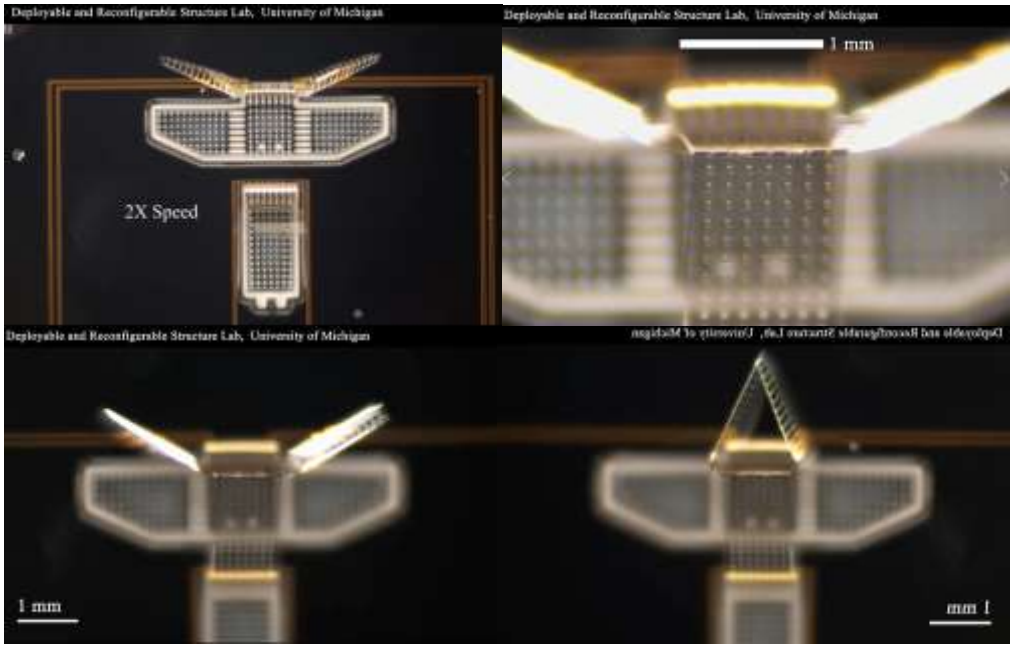

Video_S4_3DofLockingGripper

In this video, we demonstrate a micro-origami gripper with three active degrees of freedom that can lock its 3D configuration in space. This design is useful because it does not require continuous power input and is robust against fluctuation in environmental properties. To fold the pattern, we first apply current through the upper panel with locking holes and fold it to avoid contact initially. Next, we fold the bottom panel with locking pins and align the pins with the holes. We then release the current in the upper panel so that we slide the pins into the two holes and lock the structure in its 3D configuration. After the structure is locked in space, we do not need to provide continuous power input to the system. We can achieve this aligning motion because our actuator design does not rely on environmental stimuli to function. Therefore, we can control the folding motion of the upper panel and the lower panel separately to assemble the device by locking. Finally, when the structure is accurately folded, we can close the gripper by applying current through the folding circuit that controls the gripping arms.

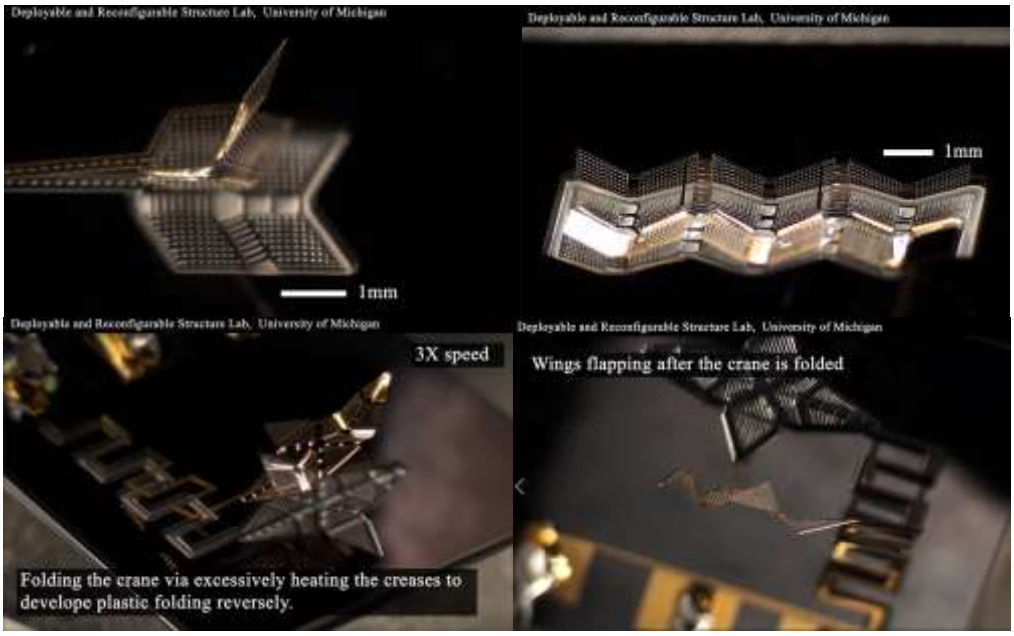

Video_S5_ComplexOri

In this video, we demonstrate two methods to create complex origami: one by combining the active and passive folds, and the other by combining the elastic and plastic folding. We first demonstrate the concept of combining the active and passive folds with a single unit Miura origami pattern and a three units Miura origami beam. Both structures can fold reversibly and rapidly by applying and removing current through the circuit. Next, we use a crane pattern to demonstrate that combining elastic and plastic folding enables us to create micro-origami that can achieve complex functions that were previously not achievable. We first apply a high voltage onto the folding circuit of the crane pattern and hold the voltage for several seconds. The plastic crease deformation is generated in the reversed direction because (1) the passive folds tend to stay flat and (2) the gravity drags the panels down. After removing the applied current, the structure returns to a folded configuration because the zero current rest angles of creases are reprogrammed. After folding the crane plastically, we can apply current through the wing circuit and flap the wings of the crane elastically. This “fold and flap wing” motion is made possible because the proposed system has multiple active degrees of freedom and uses actuators than can fold both elastically and plastically.

References for Supplementary Information

[1] MicroChem, "SU-8 2000 Permanent Epoxy Negative Photoresist," MicroChem.

[2] S. Timoshenko, "Analysis of Bi-metal thermostats," *Journal of the Optical Society of America*, 1925, 11, 233-255.

[3] J.-H. Na, A. A. Evans, J. Bae, M. C. Chiappelli, C. D. Santangelo , R. J. Lang, T. C. Hull and R. C. Hayward, "Programming reversibly self-folding origami with micropatterned photo-crosslinkable polymer trilayers," *Advanced Materials*, 2015, 27, 79-85.

[4] H. Lorenz, M. Laudon and P. Renaud, "Mechanical characterization of a new high-aspect-ratio near UV-photoresits", *Microelectron. Eng.*, 1998, 41-42, 371-374.

[5] S. P. Timoshenko and J. M. Gere, Theory of Elastic Stability (second edition), McGraw-Hill Book Company, Inc., 1986.

[6] L. L. Howell, Compliant Mechanisms, John, Wiley & Sons, Inc., 2001.

[7] K. Wouters and R. Puers, "Diffusing and swelling in SU-8: insight in material properties and processing", *J. Micromech. Microeng.*, 2010, 20, 095013.